COLLISIONAL ENERGY TRANSFER AND THE EXCITATION OF $O_2(b\,^1\Sigma_g^+)$ IN THE ATMOSPHERE†

G. WITT and J. STEGMAN

Department of Meteorology, University of Stockholm, Stockholm (Sweden)

D. P. MURTAGH, I. C. McDADE and R. G. H. GREER

Department of Pure and Applied Physics, The Queen's University of Belfast, Belfast BT7 1NN (Northern Ireland)

P. H. G. DICKINSON

Rutherford Appleton Laboratory, Chilton, Didcot, Oxon. OX11 0QX (Gt. Britain)

D. B. JENKINS

University College of Wales, Aberystwyth, Dyfed (Gt. Britain)
(Received March 5, 1984)

Summary

Optical radiation from excited oxygen species formed in the termolecular recombination of $O\,^3P$ is a permanent constituent of the planetary airglow. The emissions from the lowest singlet states of O_2 and from $O\,^1S$ are among the most conspicuous features of the terrestrial nightglow while the CO_2 atmosphere of Venus features $O_2(a\,^1\Delta_g)$ and $O_2(c\,^1\Sigma_u^-)$ as the most prominent emitters. On both planets the singlet and triplet systems are connected by a radiative transition between the $\Omega = 3$ substrate of $^3\Delta_u$ and $^1\Delta_g$.

There is increasing experimental evidence that a simple recombination scheme as the excitation source cannot properly describe the observed features of the oxygen chemiluminescence. Most of the relevant mechanisms seem to involve collisional energy transfer with O or O_2 as the transfer agent. The present work relates to a study of the $b\,^1\Sigma_g^+ \rightarrow X\,^3\Sigma_g^-$ Atmospheric Band system by rocket-borne photometry in conjunction with a parallel measurement of the oxygen atom concentration. The analysis presented below indicates that the b state is indeed excited in a two-step process with a molecular species, presumably O_2, as the transfer agent. The overall efficiency of the recombination to excite the b state is 12% - 20%. The precursor cannot, at this stage, be identified although $c\,^1\Sigma_u^-$ seems to be a plausible candidate. The precursor is quenched by both O and O_2, the ratio between the quenching coefficients ranging from 3 to 7. In conditions of dominant quenching the terrestrial $v' = 0$ bands seem to vary as $[O]^2$, independently of the pressure if a possible dependence on vibrational excitation of the precursor is neglected.

---

†Paper presented at the COSMO 84 Conference on Singlet Molecular Oxygen, Clearwater Beach, FL, U.S.A., January 4 - 7, 1984.

0047-2670/84/$3.00

1. Introduction

O_2 has six bound states known to correlate with ground state atoms. Radiative transitions from the five excited states $a^1\Delta_g$, $b^1\Sigma_g^+$, $c^1\Sigma_u^-$, $A'^3\Delta_u$ and $A^3\Sigma_u^+$ associated with the termolecular recombination of oxygen atoms are well-established features of the planetary airglow. On Earth the most intense airglow features are the $a^1\Delta_g$–$X^3\Sigma_g^-$ (IR), the $b^1\Sigma_g^+$–$X^3\Sigma_g^-$ (Atmospheric) and the vibrationally developed $A^3\Sigma_u^+$–$X^3\Sigma_g^-$ (Herzberg I) systems. The presence of the higher vibrational levels of the less conspicuous $c^1\Sigma_u^-$–$X^3\Sigma_g^-$ (Herzberg II) and $A'^3\Delta_u(\Omega = 3)$–$a^1\Delta_g$ (Chamberlain) systems has only recently been conclusively established [1 - 3]. In the predominantly CO_2 atmosphere of Venus, however, the vibrationally relaxed Herzberg II and Chamberlain Bands and the $a^1\Delta_g$–$X^3\Delta_g^-$ transition are the dominating airglow features and the Atmospheric Band system is not observed. Another important feature of the terrestrial airglow is the forbidden [OI] $^1D \leftarrow {}^1S$ "green line" at 557.7 nm also generated by oxygen atom recombination [4]. It would appear to be simple to predict the partitioning of the recombination energy of 5.21 eV among the recombination products and the dependence of the intensity and spectral shape of the emission on the reactant concentration. However, there is increasing evidence that the simple reaction scheme

$O^3P_{j_1} + O^3P_{j_2} \rightleftharpoons [O_2^*]$	primary step	(1a)
$[O_2^*] + M \longrightarrow O_2^{**}(v')$	stabilization	(1b)
$O_2^{**}(v') + M \longrightarrow O_2^*(v' - 1) + M$	vibrational quenching	(2a)
$O_2^{**}(v') + O_2 \longrightarrow O_2^{***}(v'') + O_2$	energy transfer	(2b)
$O_2^{**}(v') + O^3P \longrightarrow O_2^{***}(v'') + O^3P$ or $O_2 + O^*$		(2c)
$O_2^{**}(v') + O^* \longrightarrow O_2^{***}(v'') + O^3P$ or $O_2 + O^{**}$		(2d)
$O_2^{**}(v') \longrightarrow O_2(v'')$ or $O_2^{***}(v'') + h\nu$	radiation	(3)

where the asterisks denote one of the five excited states, comprises steps which are still insufficiently understood to permit the definitive identification of the excitation pathways. It is now believed that collisional energy transfer via an excited complex plays a significant role in the redistribution of the recombination energy. Table 1 is an attempt to summarize the more important interactions between O and O_2 with those processes specifically important to singlet O_2 identified by a frame.

The understanding of airglow mechanisms is of prime aeronomic importance as the optical emission features, by virtue of their dependence on the atmospheric compositions and temperature, reflect the chemical changes brought about by dynamic processes such as organized or diffusive transport and waves. Moreover, the unique conditions in the upper atmosphere which cannot be simulated elsewhere permit measurements complementary to kinetic studies in the laboratory. For this purpose, however, it is necessary to

TABLE 1

Oxygen gas phase interactions

	$X^3\Sigma_g^-$	$a^1\Delta_g$	^3P	^1D	^1S
$X^3\Sigma_g^-$	V–V	V–V	O_3 $^1A_1$ attraction	O_3 $^3B_2$ repulsion $\rightarrow b^1\Sigma$	O_3*? $k \propto \exp(-A/T)$
$a^1\Delta_g$	V–V IR Atmospheric	Pooling $\rightarrow b^1\Sigma$	O_3 repulsion	O_3 $^1B_2$ repulsion Hartley	O_3*? rapid
$b^1\Sigma_g^+$	V–V Atmospheric	Noxon	E–VT		
$c^1\Sigma_u^-$	Herzberg II	Slanger	$V \geqslant 0$: $a^1\Delta$ $\rightarrow$ $V > 2$: $O\,^1S$ $\rightarrow$		
$A'^3\Delta_u$ (Ω = 1, 2)	E–VT Herzberg III				
$A'^3\Delta_u$ (Ω = 3)		Chamberlain			
$A^3\Sigma_u^+$	E–VT Herzberg I				

V–V, vibrational–vibrational; E–VT, electronic–vibrational and translational.

measure simultaneously the airglow intensity, the reactant concentrations and if possible the temperature.

2. The $b\,^1\Sigma_g^+ - X\,^3\Sigma_g^-$ Atmospheric Band system

The Atmospheric Band system is one of the most prominent terrestrial airglow features. Under sunlit conditions, $b\,^1\Sigma_g^+$ is excited by resonant absorption of sunlight as well as by the reaction of $O\,^1D$ with O_2 [5]. In contrast with earlier belief, the b state is not accessible to ozone photolysis [6]. At night the sole excitation process involves the termolecular recombination of oxygen atoms. Laboratory measurements of the rate coefficient for this process [7, 8] have shown that recombination alone cannot account for the observed intensities. However, Young and Black noticed a significant increase when O_2 was added to the atomic oxygen flow. This led to the suggestion that an indirect process involving energy transfer via O_2 was responsible for the Atmospheric Band emission [9]. Such a mechanism could also be consistent with the altitude profile of the (0–0) band observed in earlier photometric rocket studies [10 - 12].

3. Experiment and analysis

In the present contribution a study of the Atmospheric Bands in two separate rocket campaigns, OXYGEN which took place on Esrange, Sweden (68° N; February 7, 1981), and ETON, South Uist, Scotland (57° N; March 23, 1982), is reported. The two campaigns occurred in basically different atmospheric conditions, the first during an intense stratospheric warming event and a geomagnetically quiet night within a disturbed period, the second under more normal conditions. Experiment OXYGEN involved the launching of two rocket payloads separated in time by 17 min. The first payload, carried by a Petrel rocket, was committed to the *in situ* measurement of the oxygen atom concentration. The second payload, on a Nike–Orion vehicle, carried an array of filter photometers tuned to different emission features related to oxygen. Since this experiment was carried out in the auroral zone, one photometer was used to monitor the 391.4 nm emission from N_2^+ as a measure of the flux of precipitating energetic electrons. The experiments of project ETON were distributed among seven Petrel payloads launched sequentially over a period of 2.5 h. Details of these experiments and the ETON results will be published elsewhere [13]. In this campaign the oxygen atom density was measured in two separate payloads, one near the beginning and one near the end of the sequence. This proved to be essential to the experiment as the oxygen density was found to change between consecutive measurements. The remaining set of rockets was instrumented with different combinations of airglow photometers. The present analysis is based on the emission profiles from flight P229.

The airglow emission was recorded by photometers looking along the rocket axis, each equipped with an interference filter, an objective lens to define a 4° half-angle field of view and a field lens to project the objective onto a photomultiplier cathode. The detectors were operated in the photon counting mode. The counts were sampled at a rate of 50 s^{-1} and transmitted to the ground via pulse code modulated telemetry. These raw data were then processed on a digital computer. The absolute energy calibration of the photometers was made with a National Bureau of Standards traceable quartz–iodine irradiance standard illuminating a freshly prepared MgO surface. During the flight a check of this calibration was performed near the rocket apogee using a Betalight device. This check also served as a dark count measurement. The response of the photometers to molecular bands was determined by convolving the measured wavelength response with a calculated rotational distribution appropriate to the expected temperature.

The photometer data represent the integrated sky radiance as a function of the rocket altitude. The data contain an extraterrestrial background component due to galactic light, zodiacal light and starlight, which exhibits a periodical modulation owing to the precession of the rocket. This background is measured near the apogee and subtracted from the observed radiance. Another periodical intensity variation associated with the precession is due to the varying zenith angle of the line of sight which changes the geometrical thickness of the emitting layer. This effect can be compensated for if the rocket attitude is known. Figure 1 shows the measured corrected

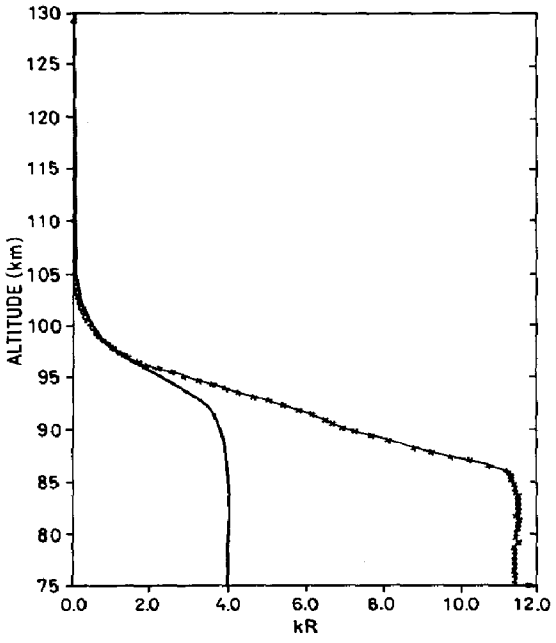

Fig. 1. Integrated overhead emission rate of the $b^1\Sigma_g^+ - X^3\Sigma_g^-$ (0–0) Atmospheric Band of O_2 at 762 nm as a function of the rocket altitude. The traces show the smoothed radiance (in kilorayleighs (kR)) from which the extraterrestrial background has been subtracted: —x—, Esrange; ——, South Uist.

profiles of the integrated overhead emission of the (0–0) Atmospheric Band recorded in the two experiments. In addition to the predictable or measurable background illumination airglow experiments may sometimes be disturbed by a contaminating light emission arising from the reaction of rocket outgassing or combustion products with ambient gas constituents. Normally such contamination is expected to occur during the descent phase when the measurement is made through the wake of the vehicle, as was observed with all the photometers in the ETON venture [14]. In experiment OXYGEN a more unusual contaminating emission was observed during ascent. As an illustration of the experimental hazards of spectrophotometry in space we show in Fig. 2 the ascent profiles of four selected emission features recorded in this study. The contaminating emission which appears to track the atomic oxygen profile is most conspicuous in the 864.5 and 724.0 nm channels. In these profiles, the contaminating emission can be immediately identified by the increase in the optical signal as the rocket ascends. In contrast, at 540 nm only a change in the slope of the profile is observed, and at 762.0 nm the contamination is even less obvious. Although the spectral composition of the contaminating emission has not yet been established, a subtraction based on judicious scaling of the 864.5 profile could be used to make both the ascent and the descent data available for analysis.

After the precession-modulated celestial background and dark emission contributions had been removed, the integrated overhead radiance was numerically differentiated to obtain the volume emission rate. The procedure adopted here for consistent smoothing and differentiation of a noisy data set is based on the Fourier transform technique. Briefly, the procedure was to create a new data set by symmetrizing the original profiles using the lowest point as a pivot, then to take the finite Fourier transform and to multiply the transform by an appropriate filter window function to remove the higher frequencies originating from small-scale fluctuations in the data and finally to perform the inverse Fourier transformation to obtain the smoothed airglow profiles. It should be noted that simply equating the amplitudes of the frequencies above a set limit to zero may give rise to a false modulation on the smoothed data and hence to artefacts in the differentiated curves. In the present analysis a Hamming [15] window which retains the lowest 20% - 40% of the Fourier frequencies was found to render acceptable profiles from which the derivative could be calculated by least-squares fitting of 1 km straight line segments over a sliding 0.5 km interval. The volume emission rate so obtained is shown in Fig. 3 for the Esrange ascent and descent profiles and the ETON ascent data. The descent data from the latter study had to be omitted from further analysis because of a chemiluminescent contamination that could not be removed from the data.

Shown on the same diagram for comparison are the profiles of the [OI] $^1D \leftarrow {}^1S$ green line volume emission recorded simultaneously with the Atmospheric Band in the two rocket flights. From this comparison it is evident that, on both occasions, the intensity maximum of the molecular emission occurred at a distinctly lower altitude than the atomic emission peak in

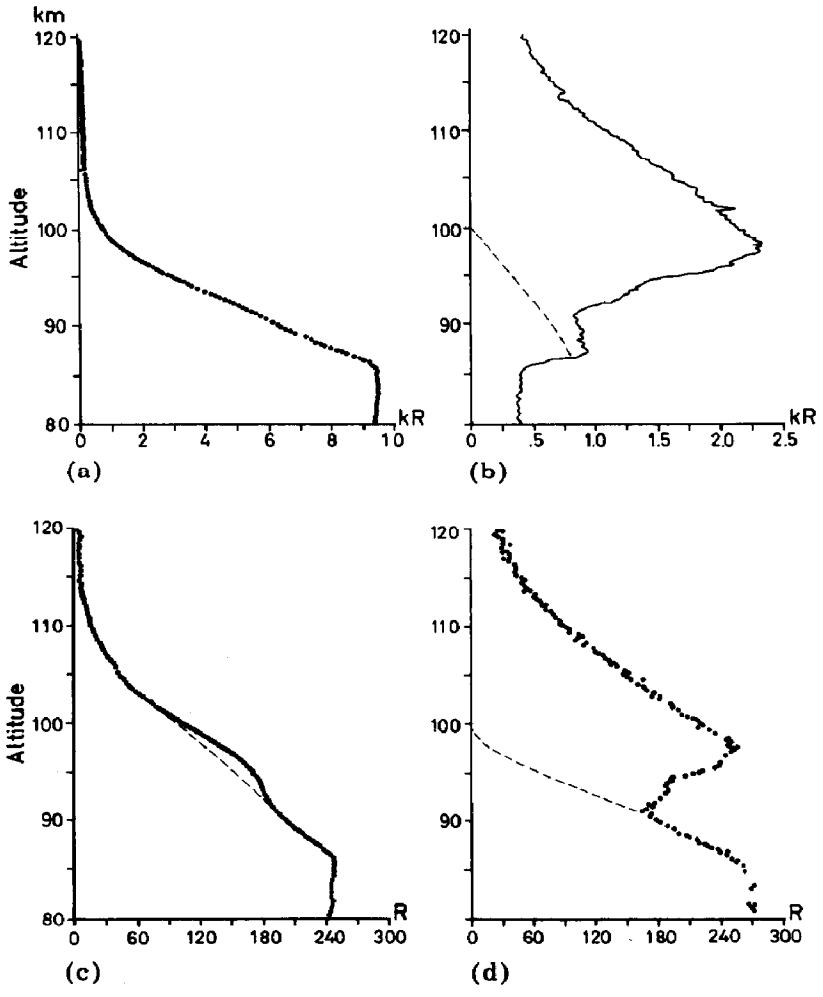

Fig. 2. Contaminating chemiluminescent emission likely to originate from the reaction of a rocket outgassing product with ambient atomic oxygen observed during the ascent phase in the Esrange experiment (February 7, 1981): (a) (0–0) Atmospheric Band of O_2 at 762 nm; (b) (0–1) O_2 Atmospheric Band at 865 nm; (c) NO + O continuum at 540 nm; (d) OH and NO + O continuum at 724 nm. The expected height variation of the emission features under study is shown by thin broken lines. The character of these features is revealed by the increase in the overhead radiance of the fainter emission features as the rocket ascends. For the stronger emissions such as the (0–0) Atmospheric Band the presence of contamination is not obvious but can be estimated using the 864.5 and 724 nm data.

accord with previous observations [10 - 12]. More importantly, in contrast with the green line the $^1\Sigma_g^+$ emission of the Esrange experiment appears to reproduce faithfully the bimodal character of the oxygen atom profile measured in a separate rocket launch 17 min before the airglow measurement. If we accept that both emission features are generated by energy transfer from a molecular metastable precursor and note the similarity in the sensitivity of $O_2(b\,^1\Sigma_g^+)$ and $O\,^1S$ to collisional electronic quenching we are

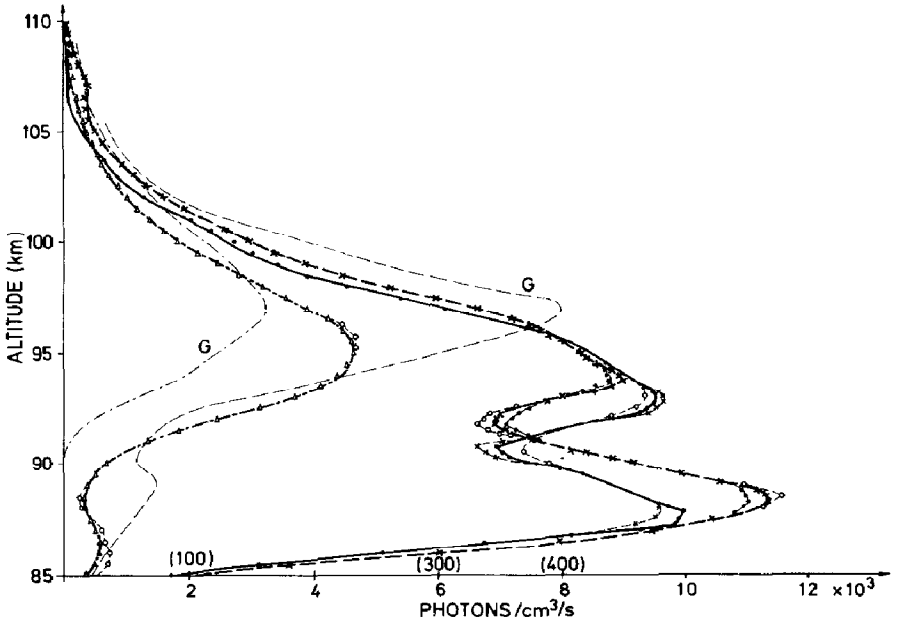

Fig. 3. Atmospheric (0–0) Band volume emission rate derived from the integrated radiance measurements by means of numerical differentiation of the smoothed recordings (the branching of the curves near the turning points shows the uncertainty associated with the choice of different smoothing intervals): ——, Esrange ascent (February 7, 1981); —x—, Esrange descent (February 7, 1981); —△—, South Uist ascent (March 23, 1982); contours G, emission profiles of the [OI] $^1D \leftarrow {}^1S$ green line also recorded in the two studies. The bimodal character of the Esrange profiles reflects a similar bimodality in the atomic oxygen concentration shown in Fig. 4. The absence of a corresponding behaviour in the green line profile should be noted.

led to the conclusion that the predominance of the molecular transition at the lower altitudes indicates that the transfer agent in this case is a molecular species. To investigate this question further we compare the observed volume emission rate I_{obs} with theoretically predicted values using the measured oxygen atom concentration as a source. Figure 4 shows the atomic oxygen profiles appropriate to the present study. The atom concentration has been determined from the fluorescent backscattering of the 130.4 nm oxygen resonance triplet generated by an on-board r.f.-powered sealed resonance lamp. This high precision measurement is brought to an absolute scale by measuring the resonant absorption along a fixed path of a fraction of the illuminating beam reflected off a corner mirror on an extended boom. The technique has been described in detail by Dickinson *et al.* [16]. Regrettably, the oxygen atom and airglow measurements were not made from the same rocket, leaving some uncertainty as to possible spatial and temporal inhomogeneities in the atom abundance. In the Esrange venture, the airglow measurement was preceded by the oxygen experiment with a time delay of 17 min while the ETON launching was bracketed by two separate oxygen atom soundings. The profile in Fig. 4 has been obtained by interpolating between these two latter measurements. For illustrative purposes, the

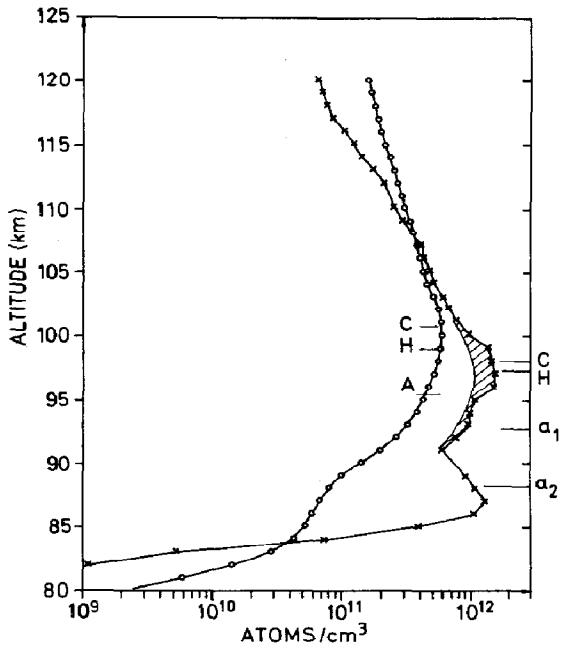

Fig. 4. Atomic oxygen concentration as a function of altitude. The measurements were made by the resonance fluorescence–absorption technique in close proximity to the airglow experiment: —x—, Esrange (February 7, 1981); —○—, South Uist (March 22, 1982) (interpolated values appropriate to the time of the airglow measurement); ▨, uncertainty in the absolute oxygen atom concentration evident from the analysis of the O_2 emissions.

positions of the intensity maxima of some of the airglow features observed in the same study ($A^3\Sigma_u^+$–$X^3\Sigma_g^-$ (Herzberg I), $A'^3\Sigma_u(\Omega = 3)$–$a^1\Sigma_g$ (Chamberlain) and the Atmospheric (0–0) Band) are indicated by horizontal lines. Profiles of the oxygen atom concentration generally exhibit a maximum between 95 and 105 km, determined by the intensity and character of vertical turbulent exchange.

Another characteristic feature of the atomic oxygen distribution is a ledge which on occasions develops into a secondary maximum below the primary peak. Such a feature is barely evidenced by the ETON data. The high latitude profile, taken under dynamic strongly disturbed conditions, exhibits this feature with an unusual intensity. Also, the peak concentration over Esrange is unusually large, in contrast with the more normal values in the ETON study. In fact, as discussed below, the measured concentration in the former experiment seems to be overestimated near the peaks. The estimated latitude of uncertainty in the upper peak of the Esrange profile is indicated in Fig. 4 by shading.

Unfortunately, a direct independent density and temperature measurement is not usually available. Therefore these parameters must be derived from an empirical model atmosphere appropriate to the season, latitude and magnetic activity with attention being paid to possible deviations during dynamically disturbed periods (*e.g.* stratospheric warming events). The

present anaysis is based on the Cospar International Reference Atmosphere [17].

The predicted emission rate I can be expressed by

$$I = \frac{k_c[O]^2[M]}{1 + \tau_b(k_1[O] + k_2[N_2])} \epsilon\eta f(z) \tag{4}$$

where k_c is the overall rate coefficient for oxygen atom recombination ($k_c = 4.7 \times 10^{-33}(300/T)^2$ cm^6 s^{-1} mol^{-2}) [18], k_1 and k_2 are the rate coefficients for electronic quenching of the b state ($k_1 = 8 \times 10^{-14}$ cm^3 s^{-1} mol^{-1} [19] and $k_2 = 2.2 \times 10^{-15}$ cm^3 s^{-1} mol^{-1} [20]) and $\tau_b = 11.5$ s is the radiative lifetime of the $b\,^1\Sigma_g^+$ state [21].

In the case of direct excitation, $\epsilon\eta f(z)$ would be the efficiency of the recombination to populate the b state, with η and $f(z)$ effectively equal to unity. For a two-step process, ϵ refers to the efficiency of excitation of the parent state and η is that of the transfer step. The height-dependent factor $f(z)$ is related to the deactivation of the precursor and, on the assumption that O_2 is the transfer agent as suggested in an earlier study [9], is given by the relationship

$$f(z) = \frac{k_4[O_2]}{A + k_3[O] + k_4[O_2] + k_5[N_2]} \tag{5}$$

where A is the radiative transition probability and k_3, k_4 and k_5 are the rate coefficients for deactivation of the parent state. Actually, expression (5) should be complemented by another height-dependent factor accounting for a possible dependence of the transfer on the vibrational excitation of the precursor which we neglect at this level of approximation. The vibrational relaxation of the $b\,^1\Sigma_g^+$ state is rapid at the densities considered [22] and, in contrast with the triplet O_2 states, no vibrational development needs to be accounted for.

Assuming that the observed emission rate is given by (4) we calculate quenching profiles defined by

$$\phi(z) = \frac{k_c[O]^2[M]}{1 + 11.5(k_1[O] + k_2[N_2])} \frac{1}{I_{obs}} \tag{6}$$

for the two cases (a) where the quenching of the b state by atomic oxygen is given by the published rate coefficient and (b) where this quenching process is disregarded. The resulting profiles derived from the ETON measurements are shown in Fig. 5. Now, for a direct excitation mechanism, $\phi(z)$ is the inverse of the excitation efficiency ϵ and remains independent of the altitude. The same would apply in the case where energy transfer is involved and the long-lived precursor is electronically quenched by the transfer agent alone. However, the traces in Fig. 5 indicate that this is not the case. Apart from the oscillations originating from a residual geometric modulation due to the rocket precession the trend of $\phi(z)$ clearly shows that the overall

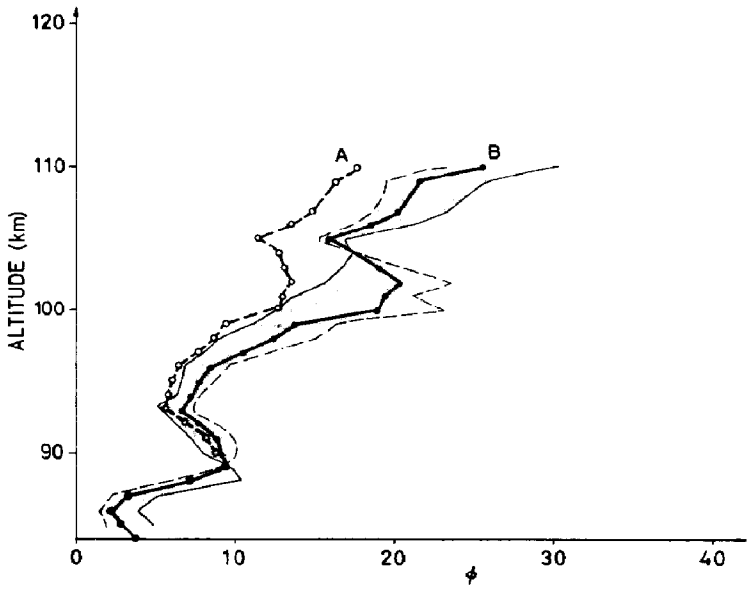

Fig. 5. Quenching profiles for the (0–0) Atmospheric Band precursor derived from the ETON measurements (the atomic oxygen concentration used in calculating ϕ was obtained by interpolation between the two oxygen measurements made before and after the airglow experiment): —○—, height variation of ϕ ($= k_c[O]^2[M]/[\{1 + \tau_b(k_1[O] + k_2[N_2])\}I_{obs}]$) for case A ($k_1 = 8 \times 10^{-14}$ cm^3 s^{-1} mol^{-1}); —●—, height variation of ϕ for case B ($k_1 = 0$). To illustrate the sensitivity of ϕ to temporal changes in the oxygen atom abundance, thin broken lines bracketing curve B show the two sets of ϕ calculated by using the actual oxygen atom concentration measurements.

excitation efficiency must decrease with altitude. Without being able at this point to identify a precursor, we consider the simplest case where the precursor is only quenched by O and O_2. Then

$$\phi(z) = \frac{A + k_3[O] + k_4[O_2]}{\epsilon\eta k_4[O_2]} \tag{7}$$

Further, if the lifetime of the precursor is long, as it would be if the parent state is indeed $c\,^1\Sigma_u^-$ as suggested by Greer *et al.* [9] the radiative decay can be neglected. Then a least-squares fitting of the constants in the expression

$$\phi(z) = \frac{1}{\epsilon\eta}\left(1 + \frac{k_3}{k_4}\frac{[O]}{[O_2]}\right) \tag{8}$$

to the data allows the determination of both ϵ and k_3/k_4. The results of the fitting depend to some extent on the height interval covered by the procedure as the volume emission rate tends to be increasingly uncertain both at the lowest altitudes where the volume emission rate is small and above about 105 km where the integrated overhead intensity has decreased to small values. The sensitivity of the analysis to variations in the oxygen atom abundance is obviously less pronounced where quenching by atomic oxygen is a significant loss of the $b\,^1\Sigma_g^+$ state.

For the ETON data set the fitted parameters are $\epsilon\eta = 0.12$ - 0.2 and $k_3/k_4 = 3$ - 7. For this simple case, where the possible dependence of the energy transfer on the vibrational distribution of the precursor has been neglected, $I \propto [O]^2$ in the limiting case of molecular quenching. At the opposite extreme where the molecular contribution to the quenching of the b state becomes small the intensity is expected to vary as $[O]^2[M]/\{1 + (k_3/k_4)([O]/[O_2])\}$. This explains the readiness of the Atmospheric Band emission to track the oxygen atom concentration in the 85 - 90 km region. Throughout the altitude region of interest the proportion of the O_2 and N_2 concentrations does not change significantly. Therefore quenching of the precursor by N_2 would affect eqn. (8) by at most an additional height-independent term in the brackets. Nevertheless, the present data are not sufficient for an analysis of the role of N_2 as an additional quencher of the b state precursor.

The analysis of the high latitude data (OXYGEN) is less simple, partly because of the presence of background contamination in both the ascent and the descent data and partly because of an uncertainty in the absolute oxygen atom density especially pronounced near the peaks. Having access to an independent measurement of the contaminating emission at 864.5 nm, we have attempted to subtract a scaled contribution from the 762 nm data assuming that the relative spectral distribution of the contaminating feature does not change with altitude. Up to about 105 km this procedure seems to be satisfactory. Above this height where the A band intensity decreases rapidly the background contribution dominates and the subtraction leads to increasing errors. Regarding the uncertainty in the oxygen atom density an independent quenching analysis of the triplet emissions recorded in the same flight furnished independent evidence that the concentration near the peaks is overestimated by as much as up to 40%. The discrepancy between the predicted and the observed quenching profiles is as expected less pronounced if the b state is quenched by atomic oxygen. The amount of mismatch is also different for the upper and lower peaks of the high latitude data. For the former, the measured oxygen atom profile can be brought to an acceptable agreement with the ETON observations, requiring only a relatively modest adjustment. For the lower peak, the mismatch is too large to be accounted for in terms of an experimental error. In consideration of the disturbed dynamic conditions prevailing at the time of the Esrange experiment it is plausible to attribute the observed discrepancy to a change in the atmospheric composition between the times of the oxygen atom and the airglow measurements.

4. Discussion and conclusions

The results presented here show clearly that the excitation of $O_2(b\,^1\Sigma_g^+)$ must proceed by a two-step mechanism involving a molecular precursor. On the basis of the experiments of Young and Black [7] and of Ogryzlo [23],

the transfer agent can be identified as ground state O_2. The present analysis also indicates that the precursor is significantly quenched by both O and O_2. However, this limited evidence is not sufficient to allow a definitive identification of the precursor. The hypothesis that the present state is $c^1\Sigma_u^-$ is not inconsistent with the airglow measurements and can to some extent be supported by the analysis of electron impact excitation of the Atmospheric Bands. Emission from $O_2(b^1\Sigma_g^+)$ is one of the brightest molecular features of the aurora [24] and considerable effort has been directed towards reconciling the observed emission intensity with the measured electron impact cross section [25]. On the basis of the experiment of Lawton and Phelps [26] who studied the excitation of the (0–0) Atmospheric Band in the interaction of low energy electrons with a pure O_2 atmosphere it has been proposed [27] that energy transfer from a metastable precursor with O_2 as the transfer agent also plays a significant role in the auroral excitation of the b state. Such a mechanism would also be required to account for the occurrence in the aurora of emissions from higher vibrational levels up to $v' = 4$ of the Atmospheric Band system [28] not accessible by the reaction

$$O_2(X^3\Sigma_g^-) + O^1D \longrightarrow O_2(b^1\Sigma_g^+) + O^3P$$

The identity of the precursor as $c^1\Sigma_u^-$ can only be hypothesized on the basis of the observed angular and energy dependence of electron scattering by O_2 [25, 29] which indicates that the production of a high-lying excited O_2 state is accompanied by a spin change. More work is obviously needed before this question can be resolved.

Acknowledgments

The authors are indebted to N. Wilhelm and P. E. Tuninger who were responsible for the design of the airglow instrumentation, to Ms. U. Jonsson who prepared the figures and to the staff of Esrange and South Uist who led the rocket campaigns to success. This research was made under grants from the Swedish Board for Space Activities and the Science and Engineering Research Council.

References

1 T. Slanger and D. L. Huestis, *J. Geophys. Res.*, *88* (1983) 4137.
2 G. Witt, J. Stegman, R. G. H. Greer and D. P. Murtagh, *EOS Abstracts, Trans. Am. Geophys. Union*, *64* (1983) 783.
3 W. E. Sharp, *EOS Abstracts, Trans. Am. Geophys. Union*, *64* (1983) 786.
4 S. Chapman, *Proc. R. Soc. London, Ser. A*, *132* (1931) 353.
5 L. Wallace and D. M. Hunten, *J. Geophys. Res.*, *73* (1968) 4813.
6 R. P. Wayne, *J. Photochem.*, *25* (1984) 345.
7 R. A. Young and G. Black, *J. Chem. Phys.*, *44* (1966) 3741.
8 R. A. Young, R. L. Sharpless and R. Stringham, *J. Chem. Phys.*, *41* (1964) 1497.

9 R. G. H. Greer, E. J. Llewellyn, B. H. Solheim and G. Witt, *Planet. Space Sci., 29* (1981) 383.
10 D. Packer, *Ann. Geophys., 17* (1961) 67.
11 A. J. Deans, G. G. Shepherd and W. F. J. Evans, *Geophys. Res. Lett., 3* (1976) 441.
12 G. Witt, J. Stegman, B. H. Solheim and E. J. Llewellyn, *Planet. Space Sci., 27* (1979) 341.
13 R. G. H. Greer, D. P. Murtagh, L. Thomas, D. B. Jenkins, P. H. G. Dickinson, D. McKinnon, E. J. Llewellyn, J. Stegman and G. Witt, submitted to *Planet. Space Sci.*
14 R. G. H. Greer, D. P. Murtagh, G. Witt and J. Stegman, in W. R. Burke (ed.), *Proc. 6th ESA Symp. on European Rocket and Balloon Program (ESA SP-183), Interlaken, 1983*, European Space Agency Scientific and Technical Publications, Noordwijk, 1983, p. 341.
15 R. B. Blackman and J. W. Tukey, *The Measurement of Power Spectra*, Dover Publications, New York, 1958.
16 P. H. G. Dickinson, W. C. Bain, L. Thomas, E. R. Williams, D. B. Jenkins and N. D. Twiddy, *Proc. R. Soc. London, Ser. A, 369* (1980) 3709.
17 *Cospar International Reference Atmosphere (CIRA 72)*, Akademie Verlag, Berlin, 1972.
18 I. M. Campbell and C. N. Gray, *Chem. Phys. Lett., 18* (1973) 607.
19 T. G. Slanger, *J. Chem. Phys., 69* (1978) 4779.
20 L. R. N. Martin, R. B. Cohen and J. R. Schatz, *Chem. Phys. Lett., 41* (1976) 394.
21 P. H. Krupenie, *J. Phys. Chem. Ref. Data, 1* (1972) 423.
22 J. F. Noxon, *J. Chem. Phys., 52* (1970) 1852.
23 E. Ogryzlo, personal communication, 1984.
24 A. Vallance Jones and R. L. Gattinger, *J. Geophys. Res., 79* (1974) 4821.
25 S. A. Trajmar, W. Williams and A. K. Kupperman, *J. Chem. Phys., 56* (1972) 3759.
26 S. A. Lawton and A. V. Phelps, *J. Chem. Phys., 69* (1978) 1055.
27 E. J. Llewellyn and B. H. Solheim, in C. S. Deehr and J. A. Holtet (eds.), *Explorations of the Polar Upper Atmosphere*, in *NATO Adv. Study Inst.*, (1980) 165.
28 R. L. Gattinger and A. Vallance Jones, *J. Chem. Phys., 81* (1976) 4789.
29 K. Wakiya, *J. Phys. B, 11* (1978) 3931.